Nanoscale

REVIEW

View Article Online
View Journal | View Issue

Cite this: *Nanoscale*, 2023, **15**, 4669

Recent progress in bio-voltage memristors working with ultralow voltage of biological amplitude

Tianda Fu,[a] Shuai Fu[b] and Jun Yao *[a,b,c]

Received 3rd December 2022,
Accepted 27th January 2023

DOI: 10.1039/d2nr06773k

rsc.li/nanoscale

Neuromorphic systems built from memristors that emulate bioelectrical information processing in the brain may overcome the limitations of traditional computing architectures. However, functional emulation alone may still not attain all the merits of bio-computation, which uses action potentials of 50–120 mV at least 10 times lower than signal amplitude in conventional electronics to achieve extraordinary power efficiency and effective functional integration. Reducing the functional voltage in memristors to this biological amplitude can thus advance neuromorphic engineering and bio-emulated integration. This review aims to provide a timely update on the effort and progress in this burgeoning research direction, covering the aspects of device material composition, performance, working mechanism, and potential application.

1. Introduction

Conventional electronics built upon CMOS technology face the challenge of sustainability due to the foreseeable physical limitations in device scaling.[1–7] The computing efficiency is further constrained by the data traffic associated with centralized (*e.g.*, von Neumann) architecture, making it more challenging to keep up with the pace of information upgrade in the big-data era.[1–7] Alternative strategies for computing have been actively sought over the past decades.[8–14] Among them, constructing neuromorphic systems that share structural and functional similarity to the biological brain, the role model of computing efficiency,[15] is considered a promising route.[2,3,16–18] A specific emphasis is to emulate the local integration of memory and logic functions in bio-computation for in-memory computing,[4,19–21] in which data is stored at the local site to reduce energy consumption and delay inherently associated with von Neumann systems. Memristors that can store the modulable (memory) state within the device are thus exploited to construct in-memory computing such as a crossbar architecture, in which the memory state is directly retrieved for vector matrix multiplication. Extensive reviews have covered the progress and prospect of memristor devices and memristor-based computing systems.[1–7,16,18–26]

While the main effort in the field has been functional development, a distinct aspect in the signal amplitude may be worth noting. Specifically, bio-computation uses action potentials of 50–120 mV (Fig. 1a),[27] whereas typical integrated memristive systems function with much higher amplitude (*e.g.*, >1 V).[22,28–30] As energy consumption has a quadratic relationship with voltage, functional emulation alone may still fall short of attaining superior energy efficiency in bio-computation. Meanwhile, a large amplitude also limits the memristive systems from effectively interfacing sensory components or even living systems for constructing intelligent systems. Reducing the functional voltage in memristors to the biological-voltage (bio-voltage) region (*e.g.*, 50–120 mV) thus carries significance for both computing and interface engineering.

[a]*Department of Electrical Computer and Engineering, University of Massachusetts, Amherst, MA 01003, USA. E-mail: juny@umass.edu*
[b]*Institute for Applied Life Sciences (IALS), University of Massachusetts, Amherst, MA 01003, USA*
[c]*Department of Biomedical Engineering, University of Massachusetts, Amherst, MA 01003, USA*

Jun Yao

Dr Jun Yao is currently a joint assistant professor in the Department of Electrical and Computer Engineering and Institute for Applied Life Sciences at the University of Massachusetts, Amherst. His research focuses on developing nanoelectronic and nanobioelectronic devices and integrated systems. He received his B.S. in Electrical Engineering and M.S. in Physics from Fudan University (China), his Ph.D. in Applied Physics from Rice University, and postdoctoral training in Chemistry and Chemical Biology at Harvard University. He is a recipient of the NSF CAREER award, Sony faculty innovation award, outstanding junior faculty award from the college, NIH Trailblazer R21 award, and Sloan Fellowship.

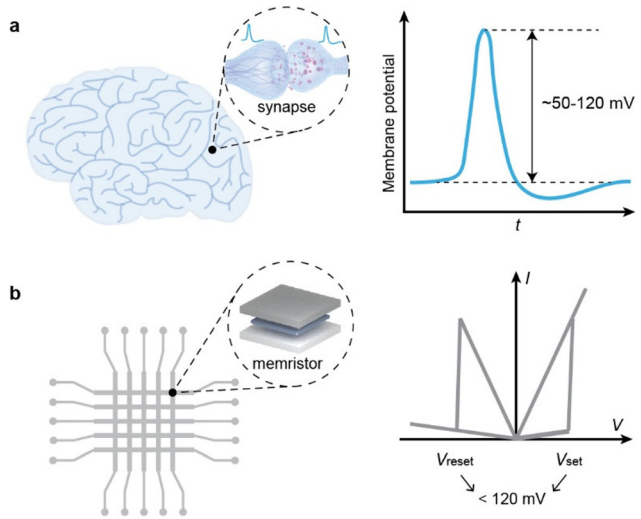

Fig. 1 Bio-voltage signal and device. (a) A biological brain uses action potentials of 50–120 mV (right) for bioelectrical computation. (b) Memristors that can be Set or Reset (right) with a voltage amplitude less than 120 mV are defined as bio-voltage memristors (BMRs).

Despite the potential implications, the development of bio-voltage memristors (BMRs), which are defined as memristors with a Set (V_{set}) or Reset (V_{reset}) voltage threshold ≤120 mV (Fig. 1b), is still at the beginning stage. Here, nonvolatile memristors with only a V_{set} or V_{reset} in the bio-voltage region are still classified as BMRs, considering that (1) the functional property and principle in half of the bio-voltage region can still be useful for device application and engineering guidance and (2) further development may enable both V_{set} and V_{reset} to fall within the bio-voltage region. In this review, we aim to provide a timely update on the progress, with the hope that it may provide a useful summary and guidance for continuous development. The review starts with discussion on typical device material composition and performance, followed by discussion of proposed enabling mechanisms. Then it extends to discussion of assembling neuromorphic components/systems by harnessing the unique properties in BMRs, concluded by discussion of future potential and challenges.

2. Materials for BMRs

Typical memristors assume a tri-layer structure with a middle dielectric layer sandwiched between two electrodes.[5,23] The electrodes often serve as not only the addressing terminals but also active components contributing to memristive behaviors.[1,7] While many conductive materials have been used as electrodes in conventional memristors, existing BMRs show a dominant preference for electrodes made from active metal elements of Ag (~70%) and Cu (~12.5%) (Fig. 2a). Previous studies show that these metals can be readily oxidized to ions, migrate across the dielectric layer, and be reduced to atoms piling up at the other electrode.[22] The continuous process yields filament formation, which bridges the two electrodes to transition the device from an initial high resistance state (HRS) to a low resistance state (LRS).[31] Facilitation of this process by the dielectric layer is considered key to reducing the functional voltage.

Among these Ag- or Cu-electrode BMRs, both inorganic materials and organic biomaterials have been used as the dielectric layers. Perovskites, such as $CsSnI_3$,[32] $CsPbI_3$,[33,34] $MAPbI_3$,[35] $Cs_3Bi_2I_9$-$CsPbI_3$,[36] and $CH_3NH_3PbI_3$,[37] have been frequently used to construct BMRs. Oxides, including SiO_2,[38] TiO,[16,39] TaO,[40–42] $Zr_{0.5}Hf_{0.5}O_2$,[43] and ITO,[44–46] are another frequent category employed as the dielectrics in BMRs. Sometimes, an oxidized interface in a non-oxide dielectric layer is also found to be key to achieving bio-voltage switching.[47] Layered two-dimensional (2D) material sheets have also been used. MoS_2 is one of the popular materials used to construct BMRs.[48–50] In addition, Lei *et al.*, reported a Ag-electrode BMR using nanosheets of bismuth oxyiodide as the dielectric layer, which achieved a V_{set} of ~50 mV.[51] Other thin semiconducting materials such as InSe[52] and GeSe[53] were also used to serve as the dielectrics in Ag-electrode and Cu-electrode BMRs, respectively.

Some BMRs do not directly use Ag or Cu electrodes but pre-introduce these elements into the dielectric layer,[54] which in effect can be considered pertaining to the same category. The elements were introduced either in a reduced metal form in composites such as Ta_2O_5-Cu,[55] AgNWs-TiO_2-PVA,[56] and

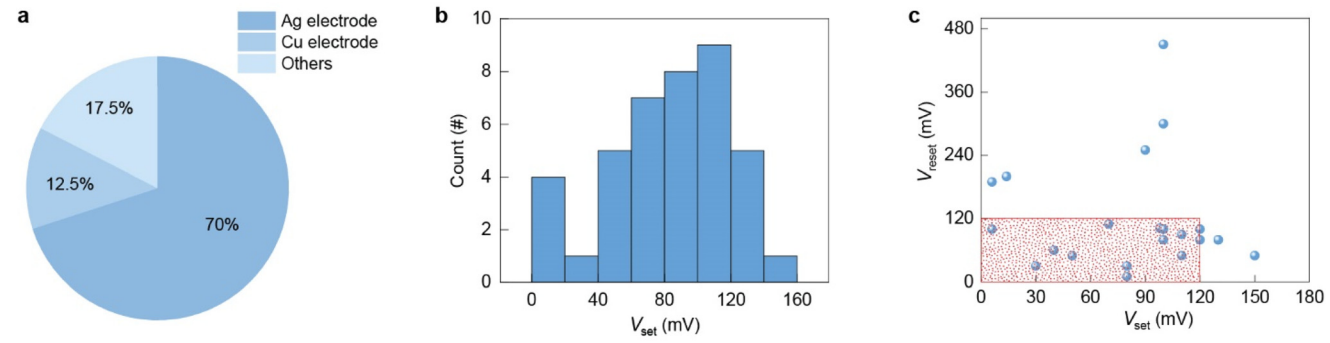

Fig. 2 Statistics of (a) electrode material composition and (b) V_{set} in both volatile and nonvolatile BMRs. (c) Distribution of V_{set} and V_{reset} in nonvolatile BMRs.

DDP-CuNPs,[54] or an oxidized ion form in compounds such as Ag_2S,[57–59] AgI,[60] and Ag_xAsS_2.[61] Pre-introduction of the elements into the dielectric layer can still facilitate voltage reduction in some BMRs already having Ag or Cu electrodes.[55–61]

Biomaterial dielectrics are not the mainstream in conventional memristors but may make a more valid argument for constructing BMRs, which may have the unique combined advantages of bio-voltage function and material biocompatibility for bio-interface implementation. A Cu-based BMR using recombinant protein rDnaJ as the dielectric achieved a V_{set} ~120 mV right at the bio-voltage boundary.[62] A V_{set} strictly falling into the bio-voltage region was realized in a Ag-based BMR employing protein nanowires as the dielectric layer.[28,63,64] These ultrasmall-diameter (*e.g.*, 3 nm) protein nanowires are outer-membrane biofilaments synthesized by the microorganism *G. sulfurreducens* living in the natural environment, so they are designed with stability for realistic device applications.[65–67] The protein-nanowire BMR achieved a V_{set} as low as 40 mV with a narrow distribution between ~40–80 mV.[28] Other Ag-based memristors using silk fibroin as the dielectric were also shown to attain bio-voltage switching under some controlled conditions.[68,69]

BMRs without the involvement of Ag or Cu elements, though much less frequent (Fig. 2a), are possible. Bio-voltage V_{set} was reported in memristors made from Au/$Rb_3Bi_2I_9$/Pt, Au/$Cs_3Bi_2I_9$/Pt, and Ti/VO_x/ITO structures.[45,70] Zhou *et al.* reported an illumination-assisted reduction of V_{set} to the bio-voltage region in a memristor based on the Au/$CH_3NH_3PbI_{3-x}Cl_x$/FTO structure.[71] In some case, a bilayer device made from the same ITO material was engineered to have a bio-voltage V_{set}.[44,46] All these memristors achieved a bio-voltage V_{set}, although the V_{reset} in some devices used to switch to HRS had values outside the bio-voltage region. The switching in them is generally attributed to field-driven modulation of defects (*e.g.*, vacancies) in the dielectric materials, although the electrodes can still facilitate the modulation through the reduction of interfacial energy barrier.

Besides BMRs constructed from conventional tri-layer solid-state materials, devices made from a biomembrane sandwiched between two aqueous solutions also exhibited bio-voltage memristive and memcapacitive behaviors.[72–76] A bio-voltage signal can induce a sufficiently high electrical field across the biomembrane due to its ultrathin thickness (*e.g.*, 3–5 nm), which is believed to change the structure (*e.g.*, through peptide insertion) or interfacing area (*e.g.*, through electrowetting) in the biomembrane for resistive or capacitive modulation, respectively. The modulation was found to be reversible, thus yielding volatile switching behaviors. The material composition in the biomembrane affected the switching dynamics such as the On/Off ratio, retention, and threshold voltage. A V_{set} as low as 25 mV was achieved.[72] Compared to conventional solid-state BMRs, biomembrane BMRs share closer features with biological organelles in structure, composition, and charge transport mechanism, which can be advantageous for creating synthetic neuromorphic components/systems in bio-realistic (*e.g.*, solution) environments. More extensive discussion of biomembrane BMRs and comparison with other biomaterial-derived devices can be found in another recent review.[77]

3. BMR performance

Retention

The retention or the time a memristor stays in a programmed state after removing the external input varies. Different retention properties can be exploited for constructing different computing functions. Several studies reported BMRs achieving retention over days or years,[35,38,62] which can be attractive for low-power data storage. However, in these studies, it is not fully clear if the nonvolatile state was actually programmed by a bio-voltage input (Table 1), since many BMRs can also operate outside the bio-voltage region and the retention can be amplitude-dependent. Some BMRs showed retention (*e.g.*, the millisecond level) falling into the temporal scale of many biological dynamics, benefiting the construction of bio-emulated dynamic functions.[28]

We may further classify a BMR into a volatile or nonvolatile one if its retention is shorter or longer than a certain time scale (*e.g.*, tens of seconds). Statistics show that the V_{set} from both types is distributed mainly in the range of 40–120 mV (Fig. 2b). A lower V_{set} in the range of several mV was observed in Cu-based BMRs using Pt/DDP-CuNPs/Au[54] and Au/Cu/ZnO-ZnS/ZnS/Pt/Ti[47] structures. The former showed volatile properties with the 4 mV V_{set}, while the latter showed the feasibility of achieving nonvolatility with a larger V_{set}. These BMRs may be useful for emulating sub-threshold neural activities to expand neuromorphic functions.

About half of the nonvolatile BMRs have a bio-voltage V_{set} but a V_{reset} outside the bio-voltage region (Fig. 2c). For example, BMRs based on bilayer ITO/ITO[45] and ITO/VO_x/Ti[44] structures achieved an extremely low V_{set} of 14 mV and 6 mV, respectively. However, a V_{Reset} >190 mV was needed to switch the devices to HRS. Nonvolatile BMRs with both V_{set} and V_{reset} in the bio-voltage region can be more attractive. Lei *et al.* reported a nonvolatile BMR based on the Ag/BiOI/Pt structure, which had a symmetric V_{set}/V_{reset} of +/−50 mV.[51]

Delay

The delay or the incubation time needed for the conductance change after applying programming voltage,[7] often characteristic of switching speed, varies significantly among different BMRs (Table 1). A short delay is generally preferred for developing fast computing applications, although the delay period can also encode rich dynamics and be exploited for constructing neuromorphic functions. While a sub-millisecond bio-voltage V_{set} pulse is able to elicit temporal synaptic modulation in some BMRs, the full switching from a HRS to LRS often requires a pulse width beyond milliseconds in existing reports. This can be considered a trade-off understood from the general mechanism, in which ionic transport is always involved in metallization or valence-change memristors. A

Table 1 Summary of bio-voltage memristors made from solid-state materials

Dielectric type	Device structure	Device size	$\lvert V_{set}\rvert$ (mV)	$\lvert V_{reset}\rvert$ (mV)	On/Off ratio	Cycles	Delay time	Retention time	Ref.
Bio-materials	Ag/protein nanowires/Ag	2 × 2 μm to 20 × 20 μm	60	—	10^6	10^4	13 ms (100 mV)	29 ms (100 mV, 20 ms)	28
	Ag/protein nanowires/Pt	2 × 2 μm to 20 × 20 um	65	—	10^5	100	—	—	64
	Ag/protein nanowires/Pd	10 × 10 μm	67	—	10^5	500	8.9 ms (100 mV)	50 ms (100 mV, 15 ms)	63
	Ag/silk:$AgNO_3$/Au	80 × 80 μm	100–170	—	3×10^6	100	—	220 μs (350 mV, 4 ms)[a]	68
	Ag/fibroin–AgNCs/ITO	D = 500 μm	30–350	30–100	10^7	300[a]	—	10^4 s[a]	69
	Cu/rDnaJ/Pt	30 × 30 μm	120	80	10^6	100	—	10^6 s[a]	62
Perovskites	Ag/$CsPbI_3$/Ag	Planar 200 × 200 nm	80	—	10^3	46	<1 ms (100 mV)	39.1 ms (100 mV, 2 ms)	33
	Ag/PMMA/ $CsPbI_3$/Pt	50 × 50 μm	100–180	100	10^6	300[a]	—	10^3 s[a]	34
	Ag/PMMA/$Cs_3Bi_2I_9$ −$CsPbI_3$/Pt	50 × 50 μm	110–190	90–150	3×10^8	10^3[a]	—	10^4 s[a]	36
	ITO/Ag/$MAPbI_3$/Al	500 × 500 μm	100	80	10^7	6×10^6[a]	100 ps (1.9 V)[a]	>2 years[a]	35
	Ag/PMMA/$CsSnI_3$/Pt	50 × 50 μm	130	80	10^3	600[a]	—	7×10^3 s[a]	32
	Au/$Rb_3Bi_2I_9$/Pt	—	90	250	2.9×10^7	200[a]	—	10^3 s[a]	70
	Au/$Cs_3Bi_2I_9$/Pt	—	100	300	9.5×10^7	400[a]	—	10^3 s[a]	70
	Ag/$CH_3NH_3PbI_3$ /Pt	50 × 50 μm	110–130	50–130	10^6	350[a]	—	1.1×10^4 s[a]	37
	Au/$CH_3NH_3PbI_{3-x}Cl_x$ /FTO	D = 200 μm	100	450	10^4	400[a]	—	13 H[a]	71
Layered 2D materials	Ag/BiOI/Pt	10 × 25 μm	50	50	10^5	50[a]	—	2×10^4 s[a]	51
	Ag/InSe/Au	50 × 50 μm	120–250	40–90	10^5	400[a]	—	—	52
	Al/Cu/Ti/MoS_2/Pt	10 × 10 μm	150–200	50–150	100	7×10^8[a]	—	—	49
	Ag/MoS_2/Ag	—	66	98	10^3	10^3[a]	—	—	48
	Ag/MoS_x/MoS_2/Ag	130 × 170 μm	100–200	100	10^6	3×10^4[a]	—	10^4 s[a]	50
	Cu/$Ge_{0.3}Se_{0.7}$/Pt	D = 150–1130 μm	50	100	200	10^4[a]	—	—	53
Metal oxides	Ti/VO_x/ITO	D = 180 μm	6–50	190–380	10	110	—	10^4 s[a]	44
	ITO/ITO	30 × 30 μm	14–18	200–500	50	100	—	10^3 s[a]	45
	Ag/TaO_x/TaO_y/Pt	D = 50 μm	110	60	10^8	100	75 ns (2 V)[a]	—	40
	Ag/TaO_x/TaO_y/TaO_x/Ag	D = 50 μm	90–180	—	10^{10}	10^6[a]	75 ns (3 V)[a]	500 ns (3 V, 5μs)[a]	41
	Ag/TaO_x/Pt	D = 500 μm	40–90	10–60	10^3	1.5×10^3[a]	100 ns (0.2 V)[a]	—	42
	Au/Cu/ZnO-ZnS/ZnS/ Pt/Ti	D = 100 μm	6	100	25	200, 1500[a]	—	10^6 s[a]	47
	Ag/TiO_xF_y/Ti/Pt	D = 200–500 μm	70	110	10^4	300[a]	100 ms (70 mV)	10 H[a]	39
	Ag/ZHO/GOQDs /ZHO/Pt	D = 100 μm	80–300	10–140	10^4	10^6[a]	14 ns (2 V)[a]	10^4 s[a]	43
	ITO/ITO(O_2)/TiN	—	40–60	60–180	10	10^7[a]	—	2×10^4 s[a]	46
	Ag/$Li_4Ti_5O_{12}$/Ag	D = 50 μm	60	—	10^8	—	150 ns (2 V)[a]	3 μs (2 V, 20 μs)[a]	16
	Ag/SiO_2/Pt	15 × 15 nm	120	100	6×10^5	5×10^4[a]	7.5 ns (1 V)[a]	6 weeks[a], 40 μs (1.4 V, 20 μs)[a]	38
Ag/Cu-based	Pt/DDP-CuNPs/Au	50 nm^2	4	0.5	10^3	100, 600[a]	—	—	54
	Cu/Ta_2O_5-Cu/PTCDA/Pt	50 × 50 μm	130	80	10^5	—	—	10 years[a]	55
	Ag/AgNWs-TiO_2 in PVA/ Pt	D = 100–500 μm	98	102	10^6	10^4[a]	—	10^6 s[a]	56
	Ag/Ag_xAsS_2/Pt	AFM Tip	70–100	100	100	—	—	—	61
	Ag/Ag_2S/Ag	STM Tip	50–100	90	2	—	—	—	57
	Ag/Ag_2S/Pt	STM Tip	90	20	200	—	—	—	58
	Ag/AgI/Pt	2 × 2 μm to 10 × 10 μm	80	20	10^3	—	30 ns (2 V)[a]	—	60
	Ag/Ag_2S/nano gap/Pt	—	80	30	10	—	—	—	59

[a] Performance was not tested by the bio-voltage signal or testing conditions were not mentioned.

reduced voltage amplitude or a reduced electric field can prolong the ionic transport.

Concomitant voltage-dependent switching dynamics are generally observed in many filamentary memristors,[22] with the Set delay decreasing in an approximately exponential manner with the increase of the input voltage amplitude. This trend was also observed in many BMRs that can also operate outside the bio-voltage region. For example, the delay in a protein-nanowire-based BMR was reduced from ~10 ms with a 100 mV input to ~0.2 ms with a 500 mV input.[63] A short delay of ~100 ns was indicated in a Ag/TaO_x/Pt BMR operating with a voltage of 200 mV close to but still larger than the bio-voltage value.[42] Other studies did not report the delay using a bio-voltage input, but showed an even shorter delay in the nanosecond or even sub-nanosecond region[35] by using input amplitude >1 V.[38] These current results show that it can be challenging to

realize fast switching in BMRs. Since ionic diffusivity or conductivity strongly correlates to the activation energy,[78] reducing this energy through material engineering may be a way out for fast-switching BMRs. Note that although it is challenging to obtain a fast Set process with a bio-voltage V_{set}, a fast Reset process (*e.g.*, ~100 ns) using bio-voltage V_{reset} of −120 mV was possible in a Al/Cu/Ti/MoS_2/Pt structure.[49] This is because the Reset process can be mainly driven by thermal effect for the rupture of filament without the ionic transport.

Memristive states

The majority of the BMRs show threshold switching with distinct LRS and HRS states. This binary switching can be implemented in digital memory, selectors, and binarized spiking neural network,[79] which may prefer a high On/Off ratio.[63,80,81] Filamentary BMRs typically achieve a high On/Off ratio (*e.g.*, $\geq 10^5$). Some BMRs made from perovskite[36,70] and oxides[16,40] were shown to achieve an On/Off ratio of ~10^8. An On/Off ratio as high as 10^{10} was achieved in a BMR made from an Ag/TaO_x/TaO_y/TaO_x/Ag structure.[41]

Multistate switching is favored for constructing analog neuromorphic systems.[8,82,83] However, multistate nonvolatile BMRs have rarely been reported. Hu *et al.*, demonstrated three-state nonvolatile BMRs with the 1st and 2nd LRS programmed by a V_{set} of 6 mV and 200 mV, respectively.[47] Choi *et al.*, demonstrated five programmed states in a BMR made from organolead halide perovskite[37] by modulating the compliance current under a fixed operation voltage (~125 mV) slightly larger than the bio-voltage value. The retention property in this achieved multistate conduction was still not fully revealed.

Endurance

Employing the memristive states for realistic applications requires reliability over repeated operation or endurance. Systematic study into the endurance of BMRs has been limited. Reported BMRs operating strictly in the bio-voltage region showed endurance up to 10^4.[28] Higher endurance was demonstrated in other BMRs, but the operational voltage was outside the bio-voltage region.[41,43,49] These results indicate that the conduction path may progressively drift to a more resilient configuration over time, which requires a larger amplitude/energy to alter. This can be understood from the general mechanism, in which the lower activation energy in the ionic species responsible for the bio-voltage function can also contribute to an easier (irreversible) dispersion over time. Engineering confined conduction pathways[84] in the memristor structure may improve endurance in the BMR.

Flexibility

BMRs, due to amplitude matching to the biosystem, may find more room in bio-interfaces,[10,85–88] which often require a soft/flexible form factor. The thin structure and small size of typical memristors readily enable them to accommodate certain flexibility without compromising performance. Flexible BMRs were demonstrated on substrates made from polyethylene terephthalate (PET),[35,56,62,69] polyimide (PI),[64] and polyethylene naphthalate (PEN).[50] The BMRs were shown to maintain performance under a standard bending test (*e.g.*, 10^4 cycles), suggesting tolerance to normal mechanical deformation in realistic settings.[64] It is worth noting that the switching dynamics in many memristors are affected by the environment (*e.g.*, humidity). Therefore, packaging for long-term stability in a bio-realistic environment constitutes another important factor, which has been less examined.

4. BMR mechanisms

Ag- and Cu-based metallization cells constitute the majority of BMRs. Generally, a three-step process involving metal oxidization at the anode ($M \rightarrow M^+ + e$), ion migration, and ion reduction at the cathode ($M^+ + e \rightarrow M$) is involved in the filament formation responsible for memristive switching.[28] As a result, facilitating one or more steps in the process is considered key to reducing the functional voltage.

Since ionic transport is always involved in metallization cells, concentrating the electric field by geometric engineering has been a common practice in BMRs (Fig. 3a). For example, typical memristors based on an Ag/SiO_2/Pt structure operated with voltage >0.2 V.[89,90] Cheng *et al.*, engineered a confined Ag/SiO_2/Pt memristor with an interelectrode distance of ~1 nm to attain a V_{set} ~100 mV, showing direct evidence that field concentration by geometry can be an enabling factor.[38] It can be generally understood that other than field enhancement through thickness reduction, a confined emission source (*i.e.*, electrode) can also facilitate the field enhancement.[91] In a Au/

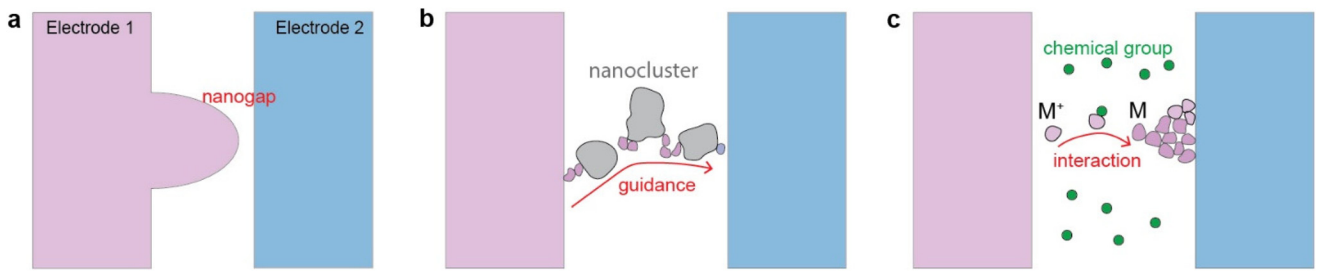

Fig. 3 Proposed mechanisms to facilitate bio-voltage switching in BMRs by (a) geometric confinement, (b) pathway guidance, and (c) chemical interaction.

Cu/ZnO-ZnS/ZnS/Pt/Ti structure,[37] Hu *et al.*, also suggested that a confined distance in the filament defined by the oxidized and unoxidized ZnS interface effectively reduced the field or voltage requirement. Along the line, 2D material layers were used to define the ultrashort interelectrode distance. Li *et al.*, used an ultrathin bilayer InSe channel (~1.6 nm thick) to fabricate Ag/InSe/Au BMR and obtained a V_{set} and V_{reset} of 120 mV and 40 mV, respectively.[52] 2D MoS_2 layers (~2 nm) were used in a Ag/MoS_2/Ag BMR to achieve both a V_{set} and V_{reset} of ~100 mV.[50] A Cu-based BMR using MoS_2 layers (2.4 nm) showed a V_{reset} as low as −50 mV, although the V_{set} was larger (150–200 mV).[49]

Under a given field, facilitating the ionic transport through microstructure engineering in the dielectric matrix constitutes another common route (Fig. 3b). Huang *et al.*, suggested that the grain boundary in the TaO_x dielectric could provide an easier pathway for Ag^+ migration;[42] reducing the granular size or increasing the grain boundary in the TaO_x dielectric in a Ag-based memristor was thus found to lower the V_{set} to the bio-voltage region. This grain-boundary mediated voltage reduction was also considered to be the enabling mechanism in a BMR fabricated from perovskite material.[36] In other cases, the introduction of intermediate nanoparticles was also considered to serve a similar role. For example, AgF nanoparticles were introduced in the TiO_xF_y dielectric in a BMR based on a Ag/TiO_xF_y/Ti/Pt structure.[39] These AgF nanoparticles were suggested to serve as passing docks to facilitate and guide Ag^+ migration. Similarly, graphene oxide quantum dots were introduced in the $Zr_{0.5}Hf_{0.5}O_2$ dielectric in a Ag-based BMR.[43] Pre-introduction of Ag or Cu nanoparticles in the dielectric can represent the similar scenario.

It is noteworthy that the above device engineering is expected to introduce different levels of defects (*e.g.*, lattice distortion, grain boundaries, or interstitial atoms) in the dielectrics. These structural defects are generally expected to lower the activation energy in the metal,[92,93] which underlies facilitation in cation transport. A correlation study is needed to determine if the activation energy (*e.g.*, to be revealed through temperature-dependent conduction measurement)[31] plays a key role in bringing down the switching threshold in BMRs. However, such a kind of investigation is scarce in existing BMR studies, which can serve as a call for future practice in the field.

Many BMRs function without the need for an ultrashort interelectrode distance or micro-engineered pathway, suggesting that the enabling mechanism can be a mixed interplay between multiple factors. Chemical interaction with the cation is also considered critical in affecting its transport and thus the voltage amplitude (Fig. 3c). Biomaterials often have innate high-density functional groups, which are also employed to construct BMRs.

Jang *et al.*, observed that the switching amplitude was closely related to the pH value of the recombinant protein rDnaj being prepared with an optimal pH ~ 6 yielding bio-voltage switching (V_{set}/V_{reset} = 120/80 mV).[62] They suggested that pH-mediated improvement of the metal (*e.g.*, Cu^+) chelation affinity to the protein was key to reducing the switching amplitude. In another case, protons in the peptide were regarded to facilitate Ag redox, although bio-voltage switching was not achieved;[94] combining other aforementioned device engineering methods (*e.g.*, geometric/microstructural engineering) may further reduce the functional voltage.

In contrast to the description of a general/overall chemical facilitation, Fu *et al.*, designed a device for the possibility of pinpointing the key enabling step.[28] They harvested biosynthetic protein nanowires from the microorganism *G. sulfurreducens to construct Ag-based memristors*. The protein nanowires are specifically designed to facilitate Ag^+ reduction. The constructed memristor could be switched with a voltage as low as 40 mV. The result suggested the facilitation in the Ag^+ cathodic reduction to be the determining step for amplitude reduction, which was further supported by experimental evidence that the protein nanowires shifted the Ag^+ reduction peak in cyclic voltammetry measurement. This proposed mechanism was also consistent with the biological function designed in the protein nanowires, although the details warrant further study.

BMRs not involving Ag or Cu filaments, though constituting a small percentage (Fig. 2a), have also been constructed. In contrast to the contribution from extrinsic Ag or Cu sources in metallization BMRs, structural change intrinsic to the dielectric layer was generally considered as the mechanism in these BMRs. In a valence-change BMR based on a Ti/VO_x/ITO structure,[44] Wang *et al.* suggested that the distribution of V_o^{2+} at the TiO_x/V interface enlarged the diffusion space, weakened the oxygen-cation bond, and generated an additional field to facilitate the migration of oxygen vacancies.[95] In a light-mediated BMR, Zhou *et al.*, proposed that light-induced holes were trapped at the perovskite/Au interface and lowered the Schottky barrier for voltage reduction.[71] Other studies considered similar mechanisms attributed to structural change in the dielectric layer. Cheng *et al.*, proposed that the tunable 1-T phase in the MoS_2 layer was responsible for the bio-voltage switching in a Ag/MoS_2/Ag structure.[48] Choi *et al.*, considered defect ions (*e.g.*, iodine vacancies) to be the key to enabling bio-voltage switching in a Ag/$CH_3NH_3PbI_3$/Pt structure.[37] It should be noted that since both types of devices involved the Ag element, the Ag-filament mechanism or combined effect may not be completely excluded. Compared to Ag and Cu cations that can independently exist in various dielectrics, these other charge species are coupled components of the dielectrics. This may explain why Ag- and Cu-based BMRs constitute the majority of BMRs (Fig. 2a).

Overall, mechanistic understanding in many BMRs is largely at the hypothetical proposal stage. As a result, detailed guidelines regarding how to engineer low-amplitude switching and improve other associated performance are lacking. This may not be too surprising because multistep processes that are further intricately correlated to defects and material properties are involved in memristive switching. Systematic mechanistic study in each device category is highly encouraged and deemed valuable for long-term development.

5. Implementation of BMRs

BMRs enable the potential of constructing neuromorphic devices that transition from mere functional emulation to also including parameter matching with neural components.[28,64] This may yield not only low-power computing[33,63] but also efficient sensor-computing interfaces.[96,97] To this end, preliminary bio-voltage neuromorphic functions have been explored with BMRs.

Artificial synapses

The plasticity in a biological synapse underlies the modulation of signal transmission, which is key to cognitive learning and memory (Fig. 4a).[98] Emulating synaptic plasticity is thus considered important for implementing hardware-based neuromorphic computing. Bio-voltage short-term plasticity (STP) and long-term plasticity (LTP) have been demonstrated with BMRs (Fig. 4b).

STP is related to short-term memory and features a temporal weight change in the timescale of a few seconds to several minutes.[99] Both nonvolatile and volatile BMRs can be used to emulate STP behaviors.[28,36,47,59] A pulsed input below the threshold input (either in duration or amplitude) of a full switching may still induce conductance change, which decays over time to yield STP. This decay can be compensated by the continuous input, depending on the frequency, to yield modulable conductance increase/decrease. Although not all BMRs were demonstrated with STP, it is believed that all should have such a property to a certain level, expected from the common competing effect between the drift and diffusion processes involved in various mechanisms. Volatile BMRs experiencing full switching can still be employed to construct a dynamic synapse by exploiting the above mechanism. Fu *et al.*, demonstrated a dynamic synapse,[28] in which the synaptic strength was dynamically modulated by the frequency of the emulated action potential input (100 mV, 1 ms) to show both paired-pulse facilitation (PPF) and paired-pulse depression (PPD).

Conversely, LTP features weight change that lasts longer (*e.g.*, >minutes).[100] Nonvolatile BMRs are thus usually employed for this functional emulation.[36,47,49,59] Kim *et al.*, demonstrated LTP, including potentiation and depression, in a synapse made from an Ag/PMMA/$(Cs_3Bi_2I_9)_{0.4}$–$(CsPbI_3)_{0.6}$/Pt structure by using a 100 mV pulse input.[36] Due to the bipolar switching in typical nonvolatile BMRs, pulses of opposite polarities were often used to emulate the presynaptic and postsynaptic signals to yield spiking timing-dependent plasticity (STDP).

The competing mechanistic picture also suggests the feasibility of the transition from STP to LTP if the constructive input rules over decay over time to build up a full conduction path, which can emulate the memory consolidation process.[101] The pulse interval is often employed as a tunable parameter to realize such a transition. Ono *et al.*, showed that reducing the pulse interval from 20 s to 2 s in a series of bio-voltage inputs (80 mV, 500 ms) yielded an STP-to-LTP transition in a synapse

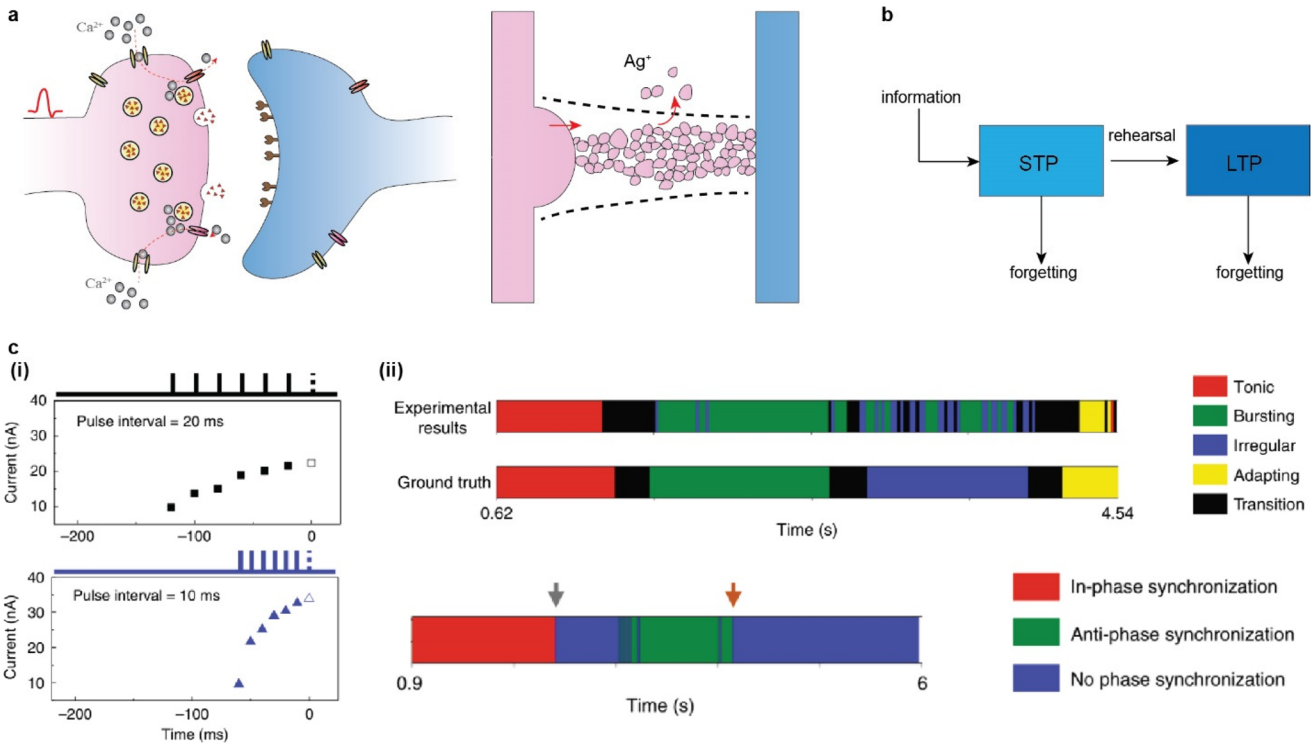

Fig. 4 Artificial synapses constructed from BMRs. (a) (Right) The flux of metal element in a filament governing the conductance change can mimic the (left) flux of Ca^{2+} in a bio-synapse underlying the plasticity. (b) A schematic of conversion from short-term plasticity (STP) to long-term plasticity (LTP). (c) (i) Synaptic evolution in a BMR stimulated with pulses of different frequencies. (ii) The synaptic BMR was employed to classify neural firing pattern. Reproduced with permission.[33] Copyright 2020, Springer Nature.

made from an Ag/Ag_2S/nanogap/Pt structure, which was employed to emulate human-memory forgetting dynamics.[59] External stimuli such as light can induce carriers to facilitate switching, which can be exploited as an additional input to modulate the STP-to-LTP transition.[51,102] Lei *et al.*, demonstrated a bio-voltage photonic synapse, in which the STP under dark conditions was elicited to LTP under light.[51]

The employment of synaptic weight for constructing a bio-voltage neural network has not yet been demonstrated. Nevertheless, the temporal dynamics in a single device can still be exploited to preprocess signals to reduce dimensionality for reservoir computing (Fig. 4c-i).[33] Specifically, the temporal distribution of the sequential spiking input is expected to yield different patterns of conductance evolution within a given time bin. This frequency-dependent synaptic behavior from a BMR based on an $Ag/CsPbI_3/Ag$ structure was exploited to pre-sort neural recordings for the efficient recognition of neural activities (Fig. 4c-ii).[33]

Artificial neurons

A neuron can be considered an independent computing unit in the sense that it has a decision (*e.g.*, firing) mechanism based on the integration of spatiotemporal inputs.[103] Artificial neurons that emulate this integrate-and-fire function can be used to construct spiking neural networks.[104,105] The incubation and spontaneous relaxation in a volatile memristor can be naturally exploited to emulate the polarization and depolarization in a neural firing.[104]

Fu *et al.*, analyzed that the dynamics of the filament formation were qualitatively similar to the dynamics of a neural firing (Fig. 5a).[28] Specifically, the net flux of the cations used for filament formation was analog to the net flux of charge in a neuron for soliciting firing, and the injected and diffusing ionic currents corresponded to the injected and leaky neuronal currents, respectively. As a result, the governing equation describing the filament formation shared a similar format to that describing the neuron model. Artificial neurons constructed from a protein-nanowire-based BMR could integrate emulated action potential (*e.g.*, 100 mV, 1 ms) and showed frequency-dependent firing consistent with the model. Importantly, the frequency dependence was found to be close to that in a real biological neuron, demonstrating the feasibility of close parameter matching with bio-computation (Fig. 5b).

The employment of artificial neurons for constructing bio-voltage spiking networks has not yet been demonstrated. Nevertheless, an individual artificial neuron with independent

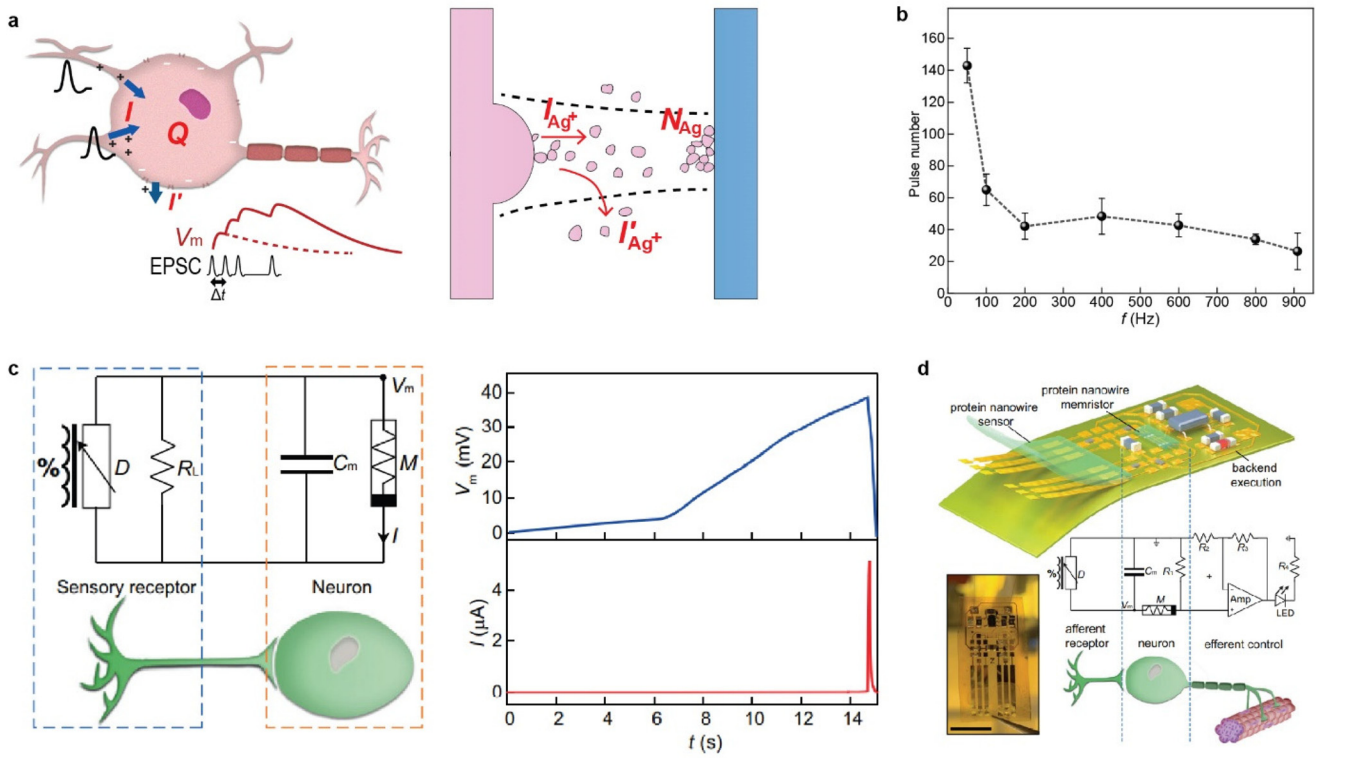

Fig. 5 Artificial neurons constructed from BMRs. (a) (Right) The ion flux in a forming filament is qualitatively analogous to (left) the charge flux in a potentiating neuron. Specifically, the injected Ag^+ current I_{Ag+}, the diffusive leaky current I'_{Ag+}, and net accumulation of Ag element (N_{Ag}) in the filamentary volume (dashed line) resemble the injected excitatory postsynaptic current (EPSC) I, leaky current through the cell membrane I', and net cytosolic charge accumulation Q, respectively. A similar governing equation can be written to describe the dynamic process. (b) An artificial neuron constructed from a protein-nanowire BMR shows frequency-dependent firing close to that in a real biological neuron. (a and b) Reproduced with permission.[28] Copyright 2020, Springer Nature. (c) An artificial neuron constructed from a protein-nanowire BMR can be directly potentiated (blue) by a bio-voltage sensing signal for firing/decision (red). (d) A wearable interface integrated with a BMR neuron that can differentiate respiratory rates. (c and d) Reproduced with permission.[64] Copyright 2021, Springer Nature.

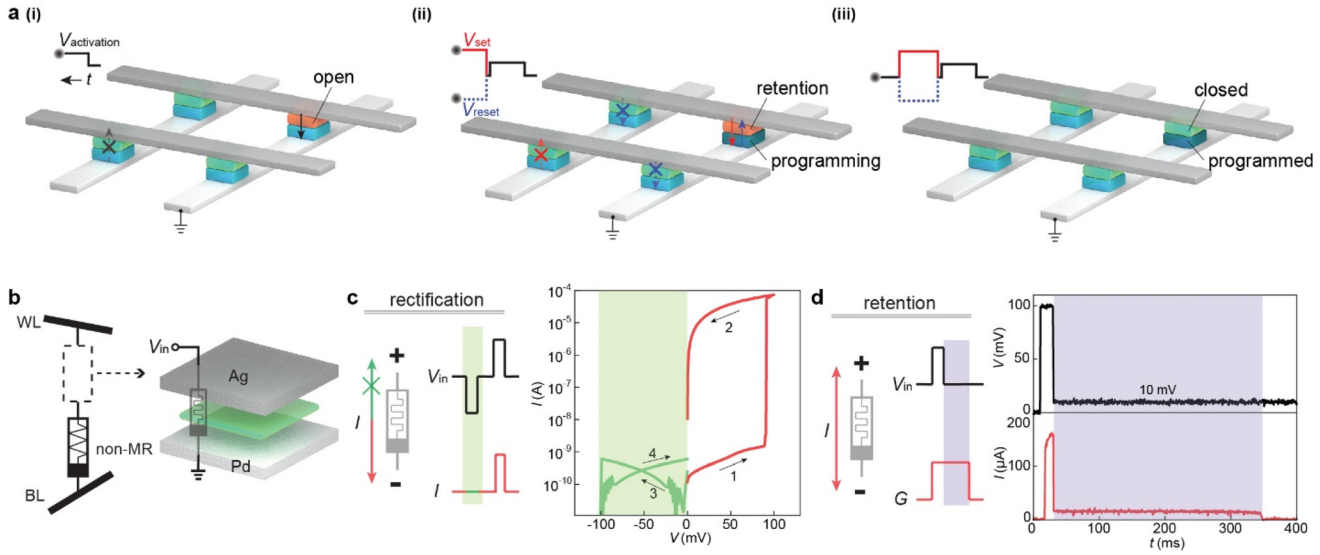

Fig. 6 An effective sneak-path solution based on a unipolar BMR with a transient retention window. (a) A schematic of the programming scheme. (i) An input ($V_{activation}$) is first applied to turn On (orange) the BMR switch in the selected path. Rest switches in the sneak path remain Off (green) due to the pinch-off switch (cross) under reverse bias. (ii) During the On retention (orange) in the selected switch, a subsequent programming voltage V_{set} or V_{reset} is directly applied to program the associated programmable nonvolatile memristor (blue). Programming in the sneak path is suppressed because it has one pinch-off switch (red cross) or two pinch-off switches (blue cross) during V_{set} or V_{reset} operation, respectively. (iii) The selected memristor assumes a different state (dark blue) after the V_{set} or V_{reset} programming pulse. The associated switch returns to Off (green) after the transient retention. (b) An Ag-protein nanowires-Pd BMR is employed to serve as the selector. The BMR features (c) a unipolar switching for rectification purpose and (d) a transient retention window for bidirectional programming. (a–d) Reproduced with permission.[63] Copyright 2022, Wiley-VCH GmbH.

decision can still be exploited for sensory information processing. The bio-voltage function can eliminate the inherent signal mismatch to sensory input, enabling the potential of direct sensor-driven computation similar to the unitary information flow in an afferent biological circuit that underlies the time and energy efficiency. Fu *et al.*, demonstrated that passive sensors[106] powered by environmental energy generated from ubiquitous ambient humidity,[107] despite the low-amplitude output, could directly drive a bio-voltage artificial neuron for decision (Fig. 5c).[64] The polarization dynamics could be further adjusted through a parallel capacitor, such that the artificial neuron was also able to do the frequency-driven computation for bodily condition (*e.g.*, respiration) monitoring (Fig. 5d).

Peripheral device

Other than serving as neural components, switching dynamics in memristors can also be used to support the construction of neural networks.[63] One such example is to exploit threshold volatile memristors as selectors to prevent the sneak path current in a neural network (Fig. 6a). Steep transitions and a high On/Off ratio are generally preferred for this selector function. However, the choice of the switching threshold (V_{th_s}) in the selector is tricky. Only when V_{th_s} is half the programming threshold (V_{th_p}) in the nonvolatile memristor, a maximal reading or analog input window ($V_{th\_p}/2$) is attained with the common half-read theme.[108] This makes the addressing theme non-generic and reduces at least half the input resolution. A BMR is thus not necessarily the optimal choice for a typical programmable memristor network using a programming threshold >0.5 V.

Fu *et al.*, developed a generic addressing theme that works with all programmable memristors and retains the full input window by exploiting the unique dynamics in a BMR (Fig. 6b).[63] Specifically, a unipolar volatile BMR was used to act like an ultra-low-threshold diode to prevent sneak path current during reading and forward (Set) programming (Fig. 6c). The transient retention offered a bidirectional window and enabled the reverse (Reset) programming needed in many bipolar programmable memristors (Fig. 6d). The strategy provides a generic solution because the activation threshold of the BMR selector is much lower than the programming thresholds in existing nonvolatile memristors. All the input shifts to the programmable memristor once the BMR selector is activated to realize the full-input utilization.

6. Summary and prospect

The BMR research is still at the very beginning stage. While existing studies have demonstrated the feasibility and potential of constructing devices/electronics functioning with bio-voltage amplitude (*e.g.*, ≤120 mV), efforts to address the associated challenges are needed to push many current proof-of-concept works towards realistic and sustainable development.

Although the bio-voltage amplitude is generally considered favorable for low-power computation, it is not the only parameter that determines energy consumption. Some filamentary

BMRs show field-driven switching and hence, a programming current lower than 1 nA can be achieved.[28,64] However, achieving a nonvolatile state typically requires a much larger programming current and longer programming time, presumably due to the fact that reaching a stable filament size requires a certain charge transport. As a result, current nonvolatile BMRs may not be favored in terms of speed and power. It is tempting to consider that engineering confined device size (*e.g.*, like that in phase change memory) to regulate the conduction path may improve power efficiency. Still, the engineering effort is preferred to be guided by the mechanistic understanding, which currently is largely at the hypothetical stage in most systems. Engineering a reliable multistate nonvolatile BMR, which is important for implementing analog neural networks, can be more challenging, as naively easing the programming (*e.g.*, with a lower activation energy) also eases the state drift.

Therefore, at present, computation based on a volatile BMR such as a spiking neural network and reservoir computing, which harness the temporal evolution and may not require a current threshold, may be a more facile direction. Importantly, reliable device performance is needed. Reports on the reliability (*e.g.*, endurance) of BMRs are scarce. The lower-amplitude switching may also be indicative of an easier dispersion in the conduction pathway and thus the tendency to fail over repeated programming. Re-activation (*e.g.*, with higher-amplitude programming) or engineering a confined conduction path may be a practical strategy for improving BMR reliability.

Neuromorphic devices and components constructed from BMRs can be a good candidate to implement in sensory interfaces. Constructing a fully self-sustained and sensor-driven intelligent system can be challenging at present, as it is tied up with the assembly of the bio-voltage computing network. Nevertheless, harnessing their low amplitude to directly preprocess sensory information can provide a realistic way to construct more efficient smart/responsive systems in real-world environments.

The potential of interfacing neuromorphic devices with biological tissue has been explored in recent studies, in which proof-of-concept demonstrations of biochemical signal processing and bioelectrical simulation was achieved.[109–111] Nevertheless, the current demonstrations required external energy input. For the long-term vision of a seamless 'cyborg' integration,[112] a self-supported energy sustainability is needed. A desirable way out is to directly use a biochemical/bioelectrical signal as the energy source for powering as well, leading to direct communication similar to the signaling pathway between cells. These neuromorphic components may be further integrated on a minimally-invasive substrate[113,114] to enable on-site, closed-loop bio-integration. Neuromorphic devices constructed from BMRs offer a unique possibility because the bio-voltage signal processing can readily match the voltage amplitude in biochemical signals (*e.g.*, resting/action potentials). Still, progress in BMR device engineering (*e.g.*, reducing power to the biological level[28] and improving reliability), bioelectronic sensor development[115] (*e.g.*, improving energy/signal retrieval), and system integration (*e.g.*, circuitry and interfacial engineering) is needed for this visionary goal.

Author contributions

T. F. and S. F. researched the data for the article. J. Y. and T. F. wrote the article. All authors contributed to the content discussion and review of the manuscript.

Conflicts of interest

There are no conflicts of interest to declare.

Acknowledgements

J. Y. acknowledges support from the National Science Foundation (DMR-2027102) and Army Research Office (W911NF2210027).

References

1 T. Shi, R. Wang, Z. Wu, Y. Sun, J. An and Q. Liu, *Small Struct.*, 2021, **2**, 2000109.
2 S. Kumar, X. Wang, J. P. Strachan, Y. Yang and W. D. Lu, *Nat. Rev. Mater.*, 2022, **7**, 575–591.
3 D. Ielmini and H.-S. P. Wong, *Nat. Electron.*, 2018, **1**, 333–343.
4 S. H. Lee, X. Zhu and W. D. Lu, *Nano Res.*, 2020, **13**, 1228–1243.
5 Z. Wang, H. Wu, G. W. Burr, C. S. Hwang, K. L. Wang, Q. Xia and J. J. Yang, *Nat. Rev. Mater.*, 2020, **5**, 173–195.
6 S. Gao, X. Yi, J. Shang, G. Liu and R.-W. Li, *Chem. Soc. Rev.*, 2019, **48**, 1531–1565.
7 R. Wang, J.-Q. Yang, J.-Y. Mao, Z.-P. Wang, S. Wu, M. Zhou, T. Chen, Y. Zhou and S.-T. Han, *Adv. Intell. Syst.*, 2020, **2**, 2000055.
8 P. Yao, H. Wu, B. Gao, J. Tang, Q. Zhang, W. Zhang, J. J. Yang and H. Qian, *Nature*, 2020, **577**, 641–646.
9 W. Wan, R. Kubendran, C. Schaefer, S. B. Eryilmaz, W. Zhang, D. Wu, S. Deiss, P. Raina, H. Qian, B. Gao, S. Joshi, H. Wu, H.-S. P. Wong and G. Cauwenberghs, *Nature*, 2022, **608**, 504–512.
10 E. J. Fuller, S. T. Keene, A. Melianas, Z. Wang, S. Agarwal, Y. Li, Y. Tuchman, C. D. James, M. J. Marinella, J. J. Yang, A. Salleo and A. A. Talin, *Science*, 2019, **364**, 570–574.
11 J. Preskill, *Quantum*, 2018, **2**, 79.
12 S. Pezzagna and J. Meijer, *Appl. Phys. Rev.*, 2021, **8**, 011308.
13 D. R. Solli and B. Jalali, *Nat. Photonics*, 2015, **9**, 704–706.
14 J. Touch, A.-H. Badawy and V. J. Sorger, *Nanophotonics*, 2017, **6**, 503–505.

15 V. Balasubramanian, *Proc. Natl. Acad. Sci. U. S. A.*, 2021, **118**, e2107022118.
16 Y. Sun, C. Song, S. Yin, L. Qiao, Q. Wan, R. Wang, F. Zeng and F. Pan, *Adv. Electron. Mater.*, 2020, **6**, 2000695.
17 W. Huh, D. Lee and C. H. Lee, *Adv. Mater.*, 2020, **32**, 2002092.
18 Y. Li, Q. Qian, X. Zhu, Y. Li, M. Zhang, J. Li, C. Ma, H. Li, J. Lu and Q. Zhang, *InfoMat*, 2020, **2**, 995–1033.
19 J. Cao, X. Zhang, H. Cheng, J. Qiu, X. Liu, M. Wang and Q. Liu, *Nanoscale*, 2022, **14**, 289–298.
20 K. Sun, J. Chen and X. Yan, *Adv. Funct. Mater.*, 2021, **31**, 2006773.
21 Y. Zhang, Z. Wang, J. Zhu, Y. Yang, M. Rao, W. Song, Y. Zhuo, X. Zhang, M. Cui, L. Shen, R. Huang and J. J. Yang, *Appl. Phys. Rev.*, 2020, **7**, 011308.
22 Z. Wang, M. Rao, R. Midya, S. Joshi, H. Jiang, P. Lin, W. Song, S. Asapu, Y. Zhuo, C. Li, H. Wu, Q. Xia and J. J. Yang, *Adv. Funct. Mater.*, 2018, **28**, 1704862.
23 D. Marković, A. Mizrahi, D. Querlioz and J. Grollier, *Nat. Rev. Phys.*, 2020, **2**, 499–510.
24 G. Ding, S.-T. Han, C.-C. Kuo, V. A. Roy and Y. Zhou, *Small Struct.*, 2022, 220015.
25 L. Gao, Q. Ren, J. Sun, S.-T. Han and Y. Zhou, *J. Mater. Chem. C*, 2021, **9**, 16859–16884.
26 S. Batool, M. Idrees, S.-R. Zhang, S.-T. Han and Y. Zhou, *Nanoscale Horiz.*, 2022, **7**, 480–507.
27 B. P. Bean, *Nat. Rev. Neurosci.*, 2007, **8**, 451–465.
28 T. Fu, X. Liu, H. Gao, J. E. Ward, X. Liu, B. Yin, Z. Wang, Y. Zhuo, D. J. Walker, J. J. Yang, J. Chen, D. R. Lovley and J. Yao, *Nat. Commun.*, 2020, **11**, 1861.
29 J. Yao, Z. Sun, L. Zhong, D. Natelson and J. M. Tour, *Nano Lett.*, 2010, **10**, 4105–4110.
30 J. Yao, L. Zhong, Z. X. Zhang, T. He, Z. Jin, P. J. Wheeler, D. Natelson and J. M. Tour, *Small*, 2009, **5**, 2910–2915.
31 Z. Wang, S. Joshi, S. E. Savel'ev, H. Jiang, R. Midya, P. Lin, M. Hu, N. Ge, J. P. Strachan, Z. Li, Q. Wu, M. Barnell, G.-L. Li, H. L. Xin, R. S. Williams, Q. Xia and J. J. Yang, *Nat. Mater.*, 2017, **16**, 101–108.
32 J. S. Han, Q. V. Le, J. Choi, H. Kim, S. G. Kim, K. Hong, C. W. Moon, T. L. Kim, S. Y. Kim and H. W. Jang, *ACS Appl. Mater. Interfaces*, 2019, **11**, 8155–8163.
33 X. Zhu, Q. Wang and W. D. Lu, *Nat. Commun.*, 2020, **11**, 2439.
34 J. S. Han, Q. V. Le, J. Choi, K. Hong, C. W. Moon, T. L. Kim, H. Kim, S. Y. Kim and H. W. Jang, *Adv. Funct. Mater.*, 2018, **28**, 1705783.
35 S. Poddar, Y. Zhang, L. Gu, D. Zhang, Q. Zhang, S. Yan, M. Kam, S. Zhang, Z. Song, W. Hu, L. Liao and Z. Fan, *Nano Lett.*, 2021, **21**, 5036–5044.
36 S. G. Kim, Q. Van Le, J. S. Han, H. Kim, M. J. Choi, S. A. Lee, T. L. Kim, S. B. Kim, S. Y. Kim and H. W. Jang, *Adv. Funct. Mater.*, 2019, **29**, 1906686.
37 J. Choi, S. Park, J. Lee, K. Hong, D. H. Kim, C. W. Moon, G. D. Park, J. Suh, J. Hwang, S. Y. Kim, H. S. Jung, N.-G. Park, S. Han, K. T. Nam and H. W. Jang, *Adv. Mater.*, 2016, **28**, 6562–6567.
38 B. Cheng, A. Emboras, Y. Salamin, F. Ducry, P. Ma, Y. Fedoryshyn, S. Andermatt, M. Luisier and J. Leuthold, *Commun. Phys.*, 2019, **2**, 28.
39 X. Sun, C. Wu, Y. Shuai, X. Pan, W. Luo, T. You, A. Bogusz, N. Du, Y. Li and H. Schmidt, *ACS Appl. Mater. Interfaces*, 2016, **8**, 32956–32962.
40 Y. Sun, C. Song, J. Yin, L. Qiao, R. Wang, Z. Wang, X. Chen, S. Yin, M. Saleem, H. Q. Wu, F. Zeng and F. Pan, *Appl. Phys. Lett.*, 2019, **114**, 193502.
41 Y. Sun, X. Zhao, C. Song, K. Xu, Y. Xi, J. Yin, Z. Wang, X. Zhou, X. Chen, G. Shi, H. Lv, Q. Liu, F. Zeng, X. Zhong, H. Wu, M. Liu and F. Pan, *Adv. Funct. Mater.*, 2019, **29**, 1808376.
42 X. Huang, K. a. Jiang, Y. Niu, R. Wang, D. Zheng, A. Dong, X. Dong, C. Mei, J. Lu, S. Liu, Z. Gan, N. Zhong and H. Wang, *Appl. Phys. Lett.*, 2018, **113**, 112103.
43 X. Yan, L. Zhang, Y. Yang, Z. Zhou, J. Zhao, Y. Zhang, Q. Liu and J. Chen, *J. Mater. Chem. C*, 2017, **5**, 11046–11052.
44 D. Wang, C. Zhang, C. Han, L. Qian and X. Huang, *J. Alloys Compd.*, 2022, **921**, 166226.
45 Y. Wang, L. Hu, X. Wei and F. Zhuge, *Appl. Phys. Lett.*, 2020, **116**, 221602.
46 C.-Y. Lin, K.-C. Chang, T.-C. Chang, T.-M. Tsai, C.-H. Pan, R. Zhang, K.-H. Liu, H.-M. Chen, Y.-T. Tseng, Y.-C. Hung, Y.-E. Syu, J.-C. Zheng, Y.-L. Wang, W. Zhang and S. M. Sze, *IEEE Electron Device Lett.*, 2015, **36**, 564–566.
47 L. Hu, S. Fu, Y. Chen, H. Cao, L. Liang, H. Zhang, J. Gao, J. Wang and F. Zhuge, *Adv. Mater.*, 2017, **29**, 1606927.
48 P. Cheng, K. Sun and Y. H. Hu, *Nano Lett.*, 2016, **16**, 572–576.
49 M. Dutta, A. Senapati, S. Ginnaram and S. Maikap, *Vacuum*, 2020, **176**, 109326.
50 A. A. Bessonov, M. N. Kirikova, D. I. Petukhov, M. Allen, T. Ryhänen and M. J. Bailey, *Nat. Mater.*, 2015, **14**, 199–204.
51 P. Lei, H. Duan, L. Qin, X. Wei, R. Tao, Z. Wang, F. Guo, M. Song, W. Jie and J. Hao, *Adv. Funct. Mater.*, 2022, **32**, 2201276.
52 Q. Li, Q. Tao, Y. Chen, L. Kong, Z. Shu, H. Duan, L. Liao and Y. Liu, *Int. J. Extreme Manuf.*, 2021, **3**, 045103.
53 C. Schindler, X. Guo, A. Besmehn and R. Waser, *Z. Phys. Chem.*, 2007, **221**, 1469–1478.
54 P. Liu, F. Hui, F. Aguirre, F. Saiz, L. Tian, T. Han, Z. Zhang, E. Miranda and M. Lanza, *Adv. Mater.*, 2022, **34**, 2201197.
55 A. Kassai and T. Hasegawa, *Jpn. J. Appl. Phys.*, 2020, **59**, SIIF01.
56 Y. Kim, W. Jeon, M. Kim, J. H. Park, C. S. Hwang and S.-S. Lee, *Appl. Mater. Today*, 2020, **19**, 100569.
57 A. Gubicza, D. Z. Manrique, L. Pósa, C. J. Lambert, G. Mihály, M. Csontos and A. Halbritter, *Sci. Rep.*, 2016, **6**, 30775.
58 J. J. Wagenaar, M. Morales-Masis and J. M. Van Ruitenbeek, *J. Appl. Phys.*, 2012, **111**, 014302.
59 T. Ohno, T. Hasegawa, T. Tsuruoka, K. Terabe, J. K. Gimzewski and M. Aono, *Nat. Mater.*, 2011, **10**, 591–595.

60 S. Tappertzhofen, I. Valov and R. Waser, *Nanotechnology*, 2012, **23**, 145703.
61 B. Zhang, P. Kutalek, P. Knotek, L. Hromadko, J. M. Macak and T. Wagner, *Appl. Surf. Sci.*, 2016, **382**, 336–340.
62 S. K. Jang, S. Kim, M. S. Salman, J.-r. Jang, Y. M. Um, L. Tan, J.-H. Park, W.-S. Choe and S. Lee, *Chem. Mater.*, 2018, **30**, 781–788.
63 T. Fu, S. Fu, L. Sun, H. Gao and J. Yao, *Adv. Mater.*, 2023, **35**, 2207133.
64 T. Fu, X. Liu, S. Fu, T. Woodard, H. Gao, D. R. Lovley and J. Yao, *Nat. Commun.*, 2021, **12**, 3351.
65 D. R. Lovley and J. Yao, *Trends Biotechnol.*, 2021, **39**, 940–952.
66 A. F. Smith, X. M. Liu, T. L. Woodard, T. D. Fu, T. Emrick, J. M. Jimenez, D. R. Lovley and J. Yao, *Nano Res.*, 2020, **13**, 1479–1484.
67 X. M. Liu, T. D. Fu, J. Ward, H. Y. Gao, B. Yin, T. Woodard, D. R. Lovley and J. Yao, *Adv. Electron. Mater.*, 2020, **6**, 2000721.
68 M. Zhao, S. Wang, D. Li, R. Wang, F. Li, M. Wu, K. Liang, H. Ren, X. Zheng, C. Guo, X. Ma, B. Zhu, H. Wang and Y. Hao, *Adv. Electron. Mater.*, 2022, **8**, 2101139.
69 K. Chang, A. Dong, X. Yu, B. Liu, X. Zhao, R. Wang, Z. Gan, K. a. Jiang, Y. Niu, X. Dong, D. Zheng, Y. Li, P. Bao, Z. Zhao and H. Wang, *Adv. Electron. Mater.*, 2022, **8**, 2100843.
70 C. Cuhadar, S.-G. Kim, J.-M. Yang, J.-Y. Seo, D. Lee and N.-G. Park, *ACS Appl. Mater. Interfaces*, 2018, **10**, 29741–29749.
71 F. Zhou, Y. Liu, X. Shen, M. Wang, F. Yuan and Y. Chai, *Adv. Funct. Mater.*, 2018, **28**, 1800080.
72 J. S. Najem, G. J. Taylor, R. J. Weiss, M. S. Hasan, G. Rose, C. D. Schuman, A. Belianinov, C. P. Collier and S. A. Sarles, *ACS Nano*, 2018, **12**, 4702–4711.
73 S. Koner, J. S. Najem, M. S. Hasan and S. A. Sarles, *Nanoscale*, 2019, **11**, 18640–18652.
74 J. S. Najem, M. S. Hasan, R. S. Williams, R. J. Weiss, G. S. Rose, G. J. Taylor, S. A. Sarles and C. P. Collier, *Nat. Commun.*, 2019, **10**, 3239.
75 J. J. Maraj, J. S. Najem, J. D. Ringley, R. J. Weiss, G. S. Rose and S. A. Sarles, *ACS Appl. Electron. Mater.*, 2021, **3**, 4448–4458.
76 W. T. McClintic, H. L. Scott, N. Moore, M. Farahat, M. Maxwell, C. D. Schuman, D. Bolmatov, F. N. Barrera, J. Katsaras and C. P. Collier, *MRS Bull.*, 2022, **47**, DOI: **10.1557/s43577-022-00344-z**.
77 M. M. Makhoul-Mansour, J. J. Maraj and S. A. Sarles, *J. Compos. Mater.*, 2022, DOI: **10.1177/00219983221135055**.
78 M. Sharma and S. Yashonath, *J. Chem. Phys.*, 2008, **129**, 144103.
79 J. K. Eshraghian, X. Wang and W. D. Lu, *IEEE Nanotechnol. Mag.*, 2022, **16**, 14–23.
80 E. Linn, R. Rosezin, C. Kügeler and R. Waser, *Nat. Mater.*, 2010, **9**, 403–406.
81 L. Zhang, S. Cosemans, D. J. Wouters, G. Groeseneken, M. Jurczak and B. Govoreanu, *IEEE Trans. Electron Devices*, 2015, **62**, 3490–3497.
82 C. Li, D. Belkin, Y. Li, P. Yan, M. Hu, N. Ge, H. Jiang, E. Montgomery, P. Lin, Z. Wang, W. Song, J. P. Strachan, M. Barnell, Q. Wu, R. S. Williams, J. J. Yang and Q. Xia, *Nat. Commun.*, 2018, **9**, 2385.
83 R. Wang, T. Shi, X. Zhang, J. Wei, J. Lu, J. Zhu, Z. Wu, Q. Liu and M. Liu, *Nat. Commun.*, 2022, **13**, 2289.
84 H. Yeon, P. Lin, C. Choi, S. H. Tan, Y. Park, D. Lee, J. Lee, F. Xu, B. Gao, H. Wu, H. Qian, Y. Nie, S. Kim and J. Kim, *Nat. Nanotechnol.*, 2020, **15**, 574–579.
85 C. Zhang, W. B. Ye, K. Zhou, H. Y. Chen, J. Q. Yang, G. Ding, X. Chen, Y. Zhou, L. Zhou, F. Li and S.-T. Han, *Adv. Funct. Mater.*, 2019, **29**, 1808783.
86 X. Zhang, Y. Zhuo, Q. Luo, Z. Wu, R. Midya, Z. Wang, W. Song, R. Wang, N. K. Upadhyay, Y. Fang, F. Kiani, M. Rao, Y. Yang, Q. Xia, Q. Liu, M. Liu and J. J. Yang, *Nat. Commun.*, 2020, **11**, 51.
87 J. H. Yoon, Z. Wang, K. M. Kim, H. Wu, V. Ravichandran, Q. Xia, C. S. Hwang and J. J. Yang, *Nat. Commun.*, 2018, **9**, 417.
88 M.-H. Kim, H.-L. Park, M.-H. Kim, J. Jang, J.-H. Bae, I. M. Kang and S.-H. Lee, *npj Flexible Electron.*, 2021, **5**, 34.
89 H. Sun, Q. Liu, C. Li, S. Long, H. Lv, C. Bi, Z. Huo, L. Li and M. Liu, *Adv. Funct. Mater.*, 2014, **24**, 5679–5686.
90 B. K. You, J. M. Kim, D. J. Joe, K. Yang, Y. Shin, Y. S. Jung and K. J. Lee, *ACS Nano*, 2016, **10**, 9478–9488.
91 B. Lepetit, D. Lemoine and M. Márquez-Mijares, *J. Appl. Phys.*, 2016, **120**, 085105.
92 R. Balluffi, *Metall. Trans. B*, 1982, **13**, 527–553.
93 B. G. Kim, S. Yeo, Y. W. Lee and M. S. Cho, *Nucl. Eng. Technol.*, 2015, **47**, 608–616.
94 M.-K. Song, S. D. Namgung, D. Choi, H. Kim, H. Seo, M. Ju, Y. H. Lee, T. Sung, Y.-S. Lee, K. T. Nam and J.-Y. Kwon, *Nat. Commun.*, 2020, **11**, 5896.
95 Z. Wang, S. Ambrogio, S. Balatti, S. Sills, A. Calderoni, N. Ramaswamy and D. Ielmini, *IEEE Trans. Electron Devices*, 2016, **63**, 4279–4287.
96 J. Chen, H. Liu, W. Wang, N. Nabulsi, W. Zhao, J. Y. Kim, M. K. Kwon and J. H. Ryou, *Adv. Funct. Mater.*, 2019, **29**, 1903162.
97 B. Tian, T. Cohen-Karni, Q. Qing, X. Duan, P. Xie and C. M. Lieber, *Science*, 2010, **329**, 830–834.
98 P. Mateos-Aparicio and A. Rodríguez-Moreno, *Front. Cell. Neurosci.*, 2019, **13**, 66.
99 J. M. Cortes, M. Desroches, S. Rodrigues, R. Veltz, M. A. Muñoz and T. J. Sejnowski, *Proc. Natl. Acad. Sci. U. S. A.*, 2013, **110**, 16610–16615.
100 Y. Yang and N. Calakos, *Front. Synaptic Neurosci.*, 2013, **5**, 8.
101 R. C. Atkinson and R. M. Shiffrin, in *Psychology of learning and motivation*, Elsevier, 1968, vol. 2, pp. 89–195.
102 X. Yang, Z. Xiong, Y. Chen, Y. Ren, L. Zhou, H. Li, Y. Zhou, F. Pan and S.-T. Han, *Nano Energy*, 2020, **78**, 105246.

103 W. Gerstner and W. M. Kistler, *Spiking neuron models: Single neurons, populations, plasticity*, Cambridge university press, 2002.
104 Z. Wang, S. Joshi, S. Savel'ev, W. Song, R. Midya, Y. Li, M. Rao, P. Yan, S. Asapu, Y. Zhuo, H. Jiang, P. Lin, C. Li, J. H. Yoon, N. K. Upadhyay, J. Zhang, M. Hu, J. P. Strachan, M. Barnell, Q. Wu, H. Wu, R. S. Williams, Q. Xia and J. J. Yang, *Nat. Electron.*, 2018, **1**, 137–145.
105 X. Zhang, W. Wang, Q. Liu, X. Zhao, J. Wei, R. Cao, Z. Yao, X. Zhu, F. Zhang, H. Lv, S. Long and M. Liu, *IEEE Electron Device Lett.*, 2017, **39**, 308–311.
106 B. Yin, X. Liu, H. Gao, T. Fu and J. Yao, *Nat. Commun.*, 2018, **9**, 5161.
107 X. Liu, H. Gao, J. E. Ward, X. Liu, B. Yin, T. Fu, J. Chen, D. R. Lovley and J. Yao, *Nature*, 2020, **578**, 550–554.
108 L. Shi, G. Zheng, B. Tian, B. Dkhil and C. Duan, *Nanoscale Adv.*, 2020, **2**, 1811–1827.
109 B. C.-K. Tee, A. Chortos, A. Berndt, A. K. Nguyen, A. Tom, A. McGuire, Z. C. Lin, K. Tien, W.-G. Bae, H. Wang, P. Mei, H.-H. Chou, B. Cui, K. Deisseroth, T. N. Ng and Z. Bao, *Science*, 2015, **350**, 313–316.
110 T. Sarkar, K. Lieberth, A. Pavlou, T. Frank, V. Mailaender, I. McCulloch, P. W. Blom, F. Torricelli and P. Gkoupidenis, *Nat. Electron.*, 2022, **5**, 774–783.
111 P. C. Harikesh, C.-Y. Yang, H.-Y. Wu, S. Zhang, M. J. Donahue, A. S. Caravaca, J.-D. Huang, P. S. Olofsson, M. Berggren, D. Tu and F. Simone, *Nat. Mater.*, 2023, **22**, 242–248.
112 R. F. Service, *Science*, 2013, **340**, 1162–1165.
113 T. G. Schuhmann Jr., J. Yao, G. Hong, T.-M. Fu and C. M. Lieber, *Nano Lett.*, 2017, **17**, 5836–5842.
114 G. Hong and C. M. Lieber, *Nat. Rev. Neurosci.*, 2019, **20**, 330–345.
115 H. Gao, F. Yang, K. Sattari, X. Du, T. Fu, S. Fu, X. Liu, J. Lin, Y. Sun and J. Yao, *Sci. Adv.*, 2022, **8**, eabn2485.